Differential Display RT–PCR Analysis of Enterovirus-71-Infected Rhabdomyosarcoma Cells Reveals mRNA Expression Responses of Multiple Human Genes with Known and Novel Functions

Peter W. F. Leong, Kingsley Liew, William Lim, and Vincent T. K. Chow[1]

Human Genome Laboratory, Department of Microbiology, Faculty of Medicine, National University of Singapore, Kent Ridge, Singapore 117597

In order to better understand cellular responses to viral infection at the transcriptional level, we employed differential display RT–PCR to analyze mRNAs from RD rhabdomyosarcoma cells following infection with a neurovirulent enterovirus 71 (EV71) strain, compared with mRNAs from uninfected cells. Of 250 expressed sequence tags (ESTs) isolated, sequenced, and identified, all were of cellular origin except 1 that was of viral origin. Of these, 156 were individual distinctive clones, comprising 45 mRNAs showing unaltered expression and 111 mRNAs exhibiting upregulation or downregulation. Of the 45 uniformly expressed mRNAs, 14 represented unknown genes. Of the 111 differentially expressed mRNAs, 63 did not match any known genes. Forty-eight of the 111 mRNAs modified by EV71 infection matched known genes, including those encoding components of cell cycle, cytoskeleton, and cell death mediators; protein degradation mediators; mitochondrial-related proteins; components of protein translation and modification; and cellular transport proteins. The altered expression profiles of representative genes were authenticated by semiquantitative RT–PCR and real-time RT–PCR. We also identified a novel alternatively spliced transcript of TRIP7 thyroid receptor interactor protein; the putative human homolog of murine mc7 mRNA predominantly expressed in the brain; and a novel mRNA similar to that encoding vacuolar protein 8 involved in protein targeting. These results underscore the applicability of the mRNA differential display technique for elucidating the expression profiles of known and even novel genes in response to cellular infection with pathogenic viruses.   © 2002 Elsevier Science (USA)

Key Words: differential display; enterovirus 71; mRNA expression; novel human genes; rhabdomyosarcoma cells; RT–PCR.

INTRODUCTION

Comprising over 100 mammalian and insect viruses, enteroviruses are a heterogeneous group of RNA viruses whose genomes consist of positive-sense, single-stranded RNA molecules that are infectious in nature. Of particular interest is enterovirus type 71 (EV71) infection, which was first described in the United States in 1974. Subsequently, several serious EV71-related outbreaks have been reported worldwide, such as those in Bulgaria (1975), Japan (1978), Australia (1986), Malaysia (1997), Taiwan (1998), and Singapore (2000) (Gilbert *et al.,* 1988; Yan *et al.,* 2000).

EV71 infection is associated with an array of clinical diseases, including hand, foot, and mouth disease (HFMD), herpangina, monoplegia, poliomyelitis-like paralysis, aseptic meningitis, encephalitis, and pulmonary edema. Among young children, EV71 is a notable cause of central nervous system disease that usually results in rapid clinical deterioration and death. Although several research studies have focused on the pathogenesis of

and immune responses to EV71, there is still a limited understanding of the molecular and cellular mechanisms of viral pathogenesis, especially pertaining to its neuro-virulence.

EV71 is rarely lethal to its host, as the virus has developed a balanced relationship with the human host whom it exploits for continuous and efficient viral replication. The virus targets the human gastrointestinal tract, in which it encounters the selection pressures of local nonspecific defences and specific gut immunity. Secondary infection of other tissues and organs is usually caused by spillover viremia and may lead to severe clinical sequelae.

The majority of viral research efforts currently focus on either viral virulence factors per se or on host defence mechanisms. However, viral-induced pathogenesis not only reflects host immune responses against virulent viruses, but is also greatly influenced by interactions between the viruses and infected cells that are accompanied by complex and dynamic changes in cellular gene expression profiles at various stages of infection. In order to gain new insights into the pathogenic consequences of virus–host cell interactions at a molecular level, we employed mRNA differential display (DD) RT–PCR (Liang and Pardee, 1992, 1995) to compare and analyze the cellular mRNA profiles of EV71-infected cells

[1] To whom correspondence and reprint requests should be addressed at Human Genome Laboratory, Department of Microbiology, Faculty of Medicine, National University of Singapore, Kent Ridge, Singapore 117597. Fax: (65) 6776-6872. E-mail: micctk@nus.edu.sg.
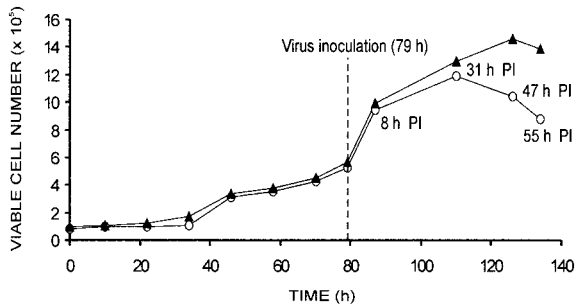
FIG. 1. Kinetics of viable cell replication of human RD rhabdomyosarcoma cells infected with EV71 at 79 h (-O-) compared with uninfected cells (-▲-). Viable cell count was assessed by the trypan blue exclusion technique. PI refers to postinfection time.

versus uninfected cells. Such an approach facilitates the characterization of known genes and the identification of novel genes that are differentially expressed or that remain unaltered in their expression during the course of EV71 infection.

RESULTS

Growth kinetics of EV71-infected RD cells

Two batches of RD cells were grown to confluency before replacing with maintenance medium containing 2% FCS. One batch of RD cells was infected with EV71 at 79 h after cell seeding, and the change in viable cell count with time was compared against that of uninfected cells. Temporal changes in cell viability were determined at 12 time points that represented various stages of cellular growth and infection. Viable growth of virus-infected cells was significantly reduced commencing from 31 h postinfection. However, only a marginal decrease in viable count of control uninfected cells was observed from 47 h postinfection, probably resulting from cell senescence (Fig. 1).

The cell counts corresponded with the inverted microscopic images of uninfected controls and EV71-infected RD cells. While the former retained their confluency, the latter displayed visible features of cytopathic effect (CPE), characterized by the rounding of cells surrounding the plaques or foci of infection. The first signs of CPE started to appear at about 31 h postinfection, progressing to moderate and advanced CPE at 47 and 55 h postinfection (data not shown).

DD RT−PCR reveals expression responses of multiple known and novel genes in RD cells infected with EV71

The mRNA expression profiles of EV71-infected RD cells at five time points at or after infection were compared by DD RT−PCR using 24 combinations of primer pairs. The results of these experiments performed in

duplicate were reproducible (Fig. 2), thereby supporting the reliability of such an approach.

Among the 250 cDNA fragments selected and sequenced, many shared overlapping sequences. Of these, 156 were individual distinctive clones comprising 45 fragments showing unaltered expression and 111 fragments exhibiting various degrees of transcriptional upregulation or downregulation. After a search of the GenBank database using the BLAST program, the cDNAs were further classified into categories based on their novelty as genes or ESTs, expression status, and cellular or viral origin (Tables 2 and 3). Of the 45 uniformly expressed mRNAs, 31 showed significant matches with the database, while 14 represented unknown genes. Of the 111 mRNAs modified by EV71 infection, 48 matched known genes; 63 of the 111 differentially expressed mRNAs did not match any known genes, of which 21 were identical to known ESTs but 42 were not found in the database.

Semiquantitative and real-time RT−PCR analyses highlight the differential expression of selected viral and cellular genes in EV71-infected RD cells

To confirm our DD RT−PCR observations on the gene expression trends with respect to time of infection, semiquantitative classical and real-time RT−PCR experiments were performed using gene-specific primers to investigate the expression profiles of 15 cellular genes and 1 viral gene (Table 1). Most of the genes analyzed by semiquantitative and real-time RT−PCR (Fig. 3) exhibited similar expression trends compared to those with DD RT−PCR (Fig. 2), with only a few genes showing slight disparities that could be attributed to the use of gene-specific primers in the former versus random primers in the latter, coupled with different thermal cycling conditions.

It was evident that the various genes were expressed at different levels during the course of viral infection, at the later stage of which a steep decline in viable cell
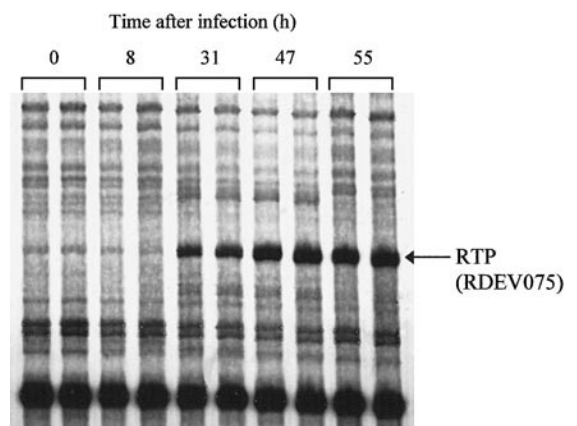

FIG. 2. A representative autoradiograph of PAGE of differential display RT−PCR products (in duplicate) showing the upregulation of RTP gene transcripts during the process of EV71 infection of RD cells.

TABLE 1

Selected Cellular and Viral Genes Whose Expression Profiles in Response to EV71 Infection Were Evaluated by Semiquantitative and Real-Time RT–PCR Using Gene-Specific Primers

| Gene | Primer sequence (5′ → 3′) | | Target size (bp) |
	Sense	Antisense	
Sarcosin	AGTCCTTACTTCTGTGAG	TCACCATTCACCTACCAG	687
MAP1B	GTGGAAGAGGTTCTCAGC	CCACTCTCAAGTAGCACT	380
hdlc1	GTAACCATGTGCGACCGA	CGTGGGCAGAAGTATGGA	506
Leukophysin	CTGCCTGTATCACTGGTC	CTACACACAGGAACTGAC	552
PSMA2	CTGTATGATGAGCGAAGT	GATGGCTGTATGAATGGC	410
PSMC2	TGATGGTGCTGGAGGTGA	TGTAACGAGGAGTAGCAC	430
COX5B	CATCTGGAGGTGGTGTTC	CTTGTAATGGGCTCCACA	268
CI-B14	TTCTACCGCCAGCACCTT	TGACTTCATGGATCGTGG	362
PiC	CTGCTGATTCTGTGGTAT	CAAGCAGATTCAGTCCAC	361
RTP	CCTCAGAACTCTTTGCTC	TCATTGCCTCTCACGCCT	374
CCT4	ACTGGTGATTGAAGAAGC	TCTTCCATTCCAGCCACA	206
Importin β	CAGGAGAGGCTAGAAGTA	CTCACACACACTCATTCT	253
RDEV154	TAAGGATGGACATTTTATCGTCTC	CAGTAAAAACACCACAGTATGCAC	166
RDEV130	GCAGGCTGGCTCTTGCTACAGA	CCTTTCGGTTATTTGGACACTATTC	285
RDEV156	CACAGTCACATTCCCTCCTTAG	TCCTGGGATAGCAGTAAATCTCTCTTACAA	162
EV71(3D)	CCAGACCATCAATTTCCA	CCTCAAGTTCTCGAAGTT	224

number was observed from the growth kinetics of infected RD cells. The expression profile of the sarcosin gene was virtually constant, implying the housekeeping function of its encoded structural protein and thereby serving as a suitable control for ensuring the inclusion of equal amounts of RNA used for the RT–PCR experiments (Fig. 3). RTP was the only gene to demonstrate an accumulation of transcripts with progression of infection. In contrast, the rest of the selected genes exhibited generally decreasing levels of expression at the later stages of infection, e.g., genes encoding leukophysin membrane protein and PSMA2 and PSMC2 protein degradation mediators (Fig. 3 and Table 2). The reduction of microtubule-associated protein 1B (MAP1B) transcripts was observed as the infection progressed. Another protein that was previously found to be associated with microtubules is dynein (Koonce and Tikhonenko, 2000). RT–PCR analysis showed a general trend of diminishing expression of the dynein light chain (hdlc1) gene during the course of infection, particularly at 47 and 55 h postinfection. Also downregulated was expression of the genes encoding mitochondrial-related proteins COX5B, NADH-ubiquinone oxidoreductase subunit CI-B14, and mitochondrial phosphate carrier (PiC), a transport protein critical in cell metabolism. Furthermore, our transcriptional profiles displayed upregulation of the tunicamycin-responsive protein (RTP) gene and downregulation of the gene encoding the chaperonin containing t-complex polypeptide (CCT4), suggestive of a pathway leading to cell death. At the later stages of infection, decreasing expression levels were demonstrated for the gene encoding importin β, one of the nuclear transport receptors

crucial for the active transport of nuclear-bound proteins (Mattaj and EngImeier, 1998).

Interestingly, we isolated only one cDNA fragment of viral origin that was homologous to the EV71 3D gene encoding RNA-dependent RNA polymerase. Although viral transcripts were not detected at 0 and 8 h after infection, these were abundant at 47 and 55 h postinfection (Fig. 3). This finding is not surprising since the virus population was expected to increase progressively during EV71 infection and corresponded with the decreasing number of viable cells. Western blot analysis of protein extracts of EV71-infected cells with anti-EV71 antiserum displayed ~37-kDa EV71 VP1 capsid protein bands (Shih *et al.,* 2000) of increasing intensity (Fig. 4), thus affirming the correlation between protein translation and gene transcription.

The RDEV154 sequence is a novel alternatively spliced variant of thyroid receptor interactor TRIP7 mRNA

The 5′ and 3′ RACE products of ~750 and ~350 bp, respectively, corresponding to the RDEV154 fragment were amplified, cloned, and sequenced. Given that both RACE products shared an overlapping region, the final connected sequence spanned 790 bp and was deposited into GenBank under Accession No. AF401520 (Fig. 5). The RDEV154 sequence produced highly significant alignments with human cDNA FLJ11501 fis clone HEMBA1002100 and with PNAS-24 mRNA that encodes a so-called apoptosis-related protein in the NB4 human acute promyelocytic leukemia cell line (GenBank Accession Nos. AK021563 and AF274949, respectively). In ad-

Gene	Classical RT-PCR expression profile	Densitometric readings					Real-time RT-PCR values				
		0	8	31	47	55	0	8	31	47	55
sarcosin		19.95	19.88	19.72	20.29	20.16	1.000	1.000	1.000	1.000	1.000
MAP1B		29.36	28.74	16.67	12.76	12.48	1.000	1.242	0.413	0.039	0.001
hdlc1		27.24	28.30	20.46	9.69	14.31	1.000	1.510	0.050	0.001	0.028
leukophysin		24.01	27.33	23.49	16.49	8.67	1.000	3.227	0.768	0.157	0.095
PSMA2		28.13	31.39	21.59	5.25	13.64	1.000	2.114	0.122	0.005	0.017
PSMC2		32.10	32.92	17.71	9.85	7.42	1.000	1.197	0.241	0.035	0.029
COX5B		28.47	27.74	25.98	5.84	11.97	1.000	1.000	0.812	0.016	0.030
CI-B14		21.07	34.98	24.65	7.29	12.01	1.000	9.849	4.199	0.391	0.895
PiC		25.95	26.55	23.89	14.34	9.27	1.000	1.662	0.859	0.463	0.269
RTP		0.00	0.00	23.97	33.65	32.68	0.000	0.000	1.000	48.04	39.84
CCT4		25.53	24.23	22.61	11.97	15.66	1.000	1.023	0.041	0.002	0.009
importin β		24.53	26.47	22.35	14.17	12.48	1.000	1.510	0.662	0.197	0.142
RDEV154		33.68	28.10	19.56	10.03	8.63	1.000	0.662	0.206	0.003	0.001
RDEV130		20.38	20.04	19.88	19.96	19.74	1.000	1.110	1.020	1.032	0.989
RDEV156		20.33	19.57	19.87	20.24	20.00	1.000	1.100	1.050	1.007	0.990
EV71(3D)		0.00	0.00	3.32	43.98	51.70	0.000	0.000	1.000	15.14	139.5

FIG. 3. Semiquantitative and real-time RT–PCR analyses of gene expression in RD cells at 0, 8, 31, 47, and 55 h following EV71 infection. Sarcosin was designated as the control housekeeping gene to normalize the samples.

dition, sequence alignment revealed that nt 22–289 and 290–465 of RDEV154 cDNA were identical to nt 16–283 and 325–500 of the thyroid receptor interactor TRIP7 cDNA (GenBank Accession No. L40357), respectively. Evident from this homology comparison was a 41-bp deletion (GTACTGCACCATCTGAAAATGGTGAAACTAAA-GCTGAAGAG) within RDEV154 cDNA that corresponded to nt 284–324 of TRIP7. Containing GT and AG boundaries, this deleted region is likely to represent an alternative exon that is alternatively spliced out via exon skipping (Chow et al., 1993; Sim and Chow, 1999). This deletion generates a frameshift mutation, and the resultant ORF is predicted to encode a 77-amino-acid RDEV154 protein with a modified and truncated C-terminus (ending with residues EN) instead of the wild-type TRIP7 protein of 99 amino acids (ending with residues APSENGETKAEEAQKTESVDNEGE). The first 32 amino acids (aa) of both proteins showed ~60% homology to human HMG-17 and included the conserved HMG motif. At aa 25–34 of both proteins was found the HMG-14 and HMG-17 DNA-binding sequence RRSARLSAR/KP that represents the consensus nucleosome core-binding domain (Alfonso et al., 1994). Proteins bearing this unique signature can be classified as members of the high-mobility group (HMG) proteins that function as transcriptional coactivators. Import of HMG proteins into the nucleus requires a bipartite nuclear localization signal (NLS). The N-terminal NLS consensus is PKRK, while the C-terminal consensus is KGKK/RG, both of which are present in TRIP7 and RDEV154 proteins. The PSORT program predicted nuclear localization for the RDEV154 protein with a high probability of 0.984. The ProtParam tool and Plot Structure program predicted a hydrophilic and unstable protein with an estimated half-life of 30 h.

RDEV154 mRNA showed a downregulated expression profile in RD cells infected with EV71 (Fig. 3). Two PCR

TABLE 2

List of 79 Isolated ESTs Showing Significant Matches with 1 Viral and 78 Human cDNAs in The Nonredundant Database

Clone ID	Approx. size (bp)	Accession No.	Description of best hit	Expression profile[a]
Viral proteins				
RDEV003	450	U22522	Enterovirus 71 MS/7423/87 complete sequence (3D protein)	↑
Components of cytoskeleton and cell death mediators				
RDEV194	450	NM_006063	Sarcomeric muscle protein (SARCOSIN), mRNA	Uniform
RDEV212	190	L06237	Microtubule-associated protein 1B (MAP1B) gene, complete cds	↓
RDEV249	560	NM_003746	Dynein, cytoplasmic, light polypeptide (PIN), mRNA	↓
Membrane proteins				
RDEV064	180	BC002392	Membrane protein, palmitoylated 1 (55 kDa), mRNA, complete cds	Uniform
RDEV086	170	U03643	Leukophysin (LKP) mRNA, complete cds	↓
RDEV208	240	U45955	Neuronal membrane glycoprotein M6b mRNA, partial cds	↓
Protein degradation mediators				
RDEV030	200	NM_002787	Proteasome (prosome, macropain) subunit, α type, 2 (PSMA2), mRNA	↓
RDEV253	480	NM_004152	Ornithine decarboxylase antizyme 1 (OAZ1), mRNA	↓
RDEV381	310	NM_002803	Proteasome (prosome, macropain) 26S subunit, ATPase, 2 (PSMC2), mRNA	↓
Mitochondrial-related proteins (respiratory)				
RDEV094	360	X55654	Mitochondrial coxII mRNA for cytochrome c oxidase II subunit	Uniform
RDEV122	220	NM_001862	Cytochrome c oxidase subunit Vb (COX5B), nuclear gene encoding mitochondrial protein, mRNA	↓
RDEV160	380	NM_002490	NADH dehydrogenase (ubiquinone) 1-α subcomplex, 6 (14 kDa, B14) (NDUFA6), mRNA	↓
RDEV199	330	X77337	Gene for phosphate carrier	↓
RDEV218	550	NM_001688	ATP synthase, H^+ transporting, mitochondrial FO complex, subunit b, isoform 1 (ATP5F1), mRNA	↓
RDEV223	450	NM_001863	Cytochrome c oxidase subunit VIb (COX6B), nuclear gene encoding mitochondrial protein, mRNA	↓
RDEV263	280	AF004342	NADH dehydrogenase III gene, mitochondrial gene encoding mitochondrial protein, partial cds	↓
RDEV367	505	AF004340	ATPase 6/8 gene, mitochondrial gene encoding mitochondrial protein, partial cds	↓
Cellular metabolism				
RDEV008	625	XM_003932	3-Hydroxy-3-methylglutaryl-coenzyme A reductase (HMGCR), mRNA	Uniform
RDEV290	750	NM_005566	Lactate dehydrogenase A (LDHA), mRNA	↓
Cell cycle and development				
RDEV015	425	AF119226	Dual-specificity tyrosine phosphatase YVH1 mRNA, complete cds	Uniform
RDEV024	250	S78234	nuc2 homolog (human, fibroblasts, mRNA, 3320 nt)	Uniform
RDEV075	310	D87953	mRNA for RTP, complete cds	↑
RDEV227	390	AF053537	p33 (ING2) mRNA, complete cds	Uniform
RDEV294	450	NM_006765	Putative prostate cancer tumor suppressor (N33), mRNA	Uniform
RDEV339	210	NM_016831	Period (*Drosophila*) homolog 3 (PER3), mRNA	↑
RDEV378	320	NM_004772	P311 protein (P311), mRNA	Uniform
Components of protein translation and modification				
RDEV016	400	NM_000972	Ribosomal protein L7a (RPL7A), mRNA	↑
RDEV079	270	XM_017838	Ribosomal protein L27a (RPL27A), mRNA	Uniform
RDEV109	420	J01415	16S ribosomal RNA, human mitochondrion, complete genome	↓
RDEV157	450	XM_010550	Ribosomal protein L7 (RPL7), mRNA	Uniform
RDEV190	550	X16869	mRNA for elongation factor 1-α (clone CEF4)	↓
RDEV225	430	NM_001006	Ribosomal protein S3A (RPS3A), mRNA	↓
RDEV278	470	AB050855	β3GalNAcT-1 mRNA for globoside synthase, complete cds, clone: type 1	Uniform
RDEV279	420	NM_001762	Chaperonin containing TCP1, subunit 6A (ζ-1) (CCT6A), mRNA	↓
RDEV292	490	NM_002717	Protein phosphatase 2 (formerly 2A), regulatory subunit B (PR 52), α isoform (PPP2R2A), mRNA	Uniform
RDEV306	260	NM_006430	Chaperonin containing TCP1, subunit 4 (δ) (CCT4), mRNA	↓
RDEV366	600	NM_001017	Ribosomal protein S13 (RPS13), mRNA	↓

TABLE 2 — *Continued*

Clone ID	Approx. size (bp)	Accession No.	Description of best hit	Expression profile[a]
Transport and traffic proteins				
RDEV054	300	AF054187	α NAC mRNA, complete cds	Uniform
RDEV152	540	AY028435	Adaptor protein kanadaptin mRNA, complete cds	Uniform
RDEV181	590	M11146	Ferritin H chain mRNA, complete cds	Uniform
RDEV228	370	L38951	Importin β subunit mRNA, complete cds	↓
Modulators of signal transduction				
RDEV027	200	U86293	Olfactory receptor (OR912-111) pseudogene, partial sequence	Uniform
RDEV126	350	XM_003950	Guanine nucleotide-binding protein (G protein), β polypeptide-2-like 1 (GNB2L1), mRNA	Uniform
Transcriptional regulators				
RDEV011	560	XM_002653	cAMP-responsive element-binding protein 1 (CREB1), mRNA	Uniform
RDEV047	380	XM_002548	Nuclear factor (erythroid-derived 2)-like 2 (NFE2L2), mRNA	Uniform
RDEV077	290	AF094481	Trinucleotide repeat DNA-binding protein p20-CGGBP gene, complete cds	Uniform
RDEV154	450	L40357	Thyroid receptor interactor (TRIP7) mRNA, 3′ end of cds	↓
RDEV241	190	AF084555	Okadaic acid-inducible and cAMP-regulated phosphoprotein 19 (ARPP-19) mRNA, complete cds	Uniform
RDEV296	420	NM_005870	sin3-associated polypeptide, 18 kDa (SAP18), mRNA	Uniform
RDEV315	190	NM_004126	Guanine nucleotide-binding protein 11 (GNG11), mRNA	↓
RDEV382	260	NM_002015	forkhead box O1A (rhabdomyosarcoma) (FOXO1A), mRNA	Uniform
Nucleic acids maintenance				
RDEV043	480	NM_002092	G-rich RNA sequence-binding factor 1 (GRSF1), mRNA	Uniform
RDEV300	370	NM_003642	Histone acetyltransferase 1 (HAT1), mRNA	↓
Miscellaneous or unknown roles				
RDEV017	360	AB029008	mRNA for KIAA1085 protein, partial cds	Uniform
RDEV033	180	NM_022774	Hypothetical protein FLJ21144 (FLJ21144), mRNA	↓
RDEV042	450	AF204869	Hemochromatosis protein (HFE) gene, promoter region and partial sequence	↑
RDEV045	390	AL117609	mRNA; cDNA DKFZp564O0463 (from clone DKFZp564O0463); partial cds	↓
RDEV046	380	NM_020357	PEST-containing nuclear protein (pcnp), mRNA	↓
RDEV071	640	NM_003295	Tumor protein, translationally controlled 1 (TPT1), mRNA	↓
RDEV130	530	AL136859	mRNA; cDNA DKFZp434P1735 (from clone DKFZp434P1735); complete cds	Uniform
RDEV135	380	NM_015380	CGI-51 protein (CGI-51), mRNA	↓
RDEV136	370	NM_018255	Hypothetical protein FLJ10879 (FLJ10879), mRNA	↑
RDEV140	310	AK025216	cDNA: FLJ21563 fis, clone COL06445	↓
RDEV144	210	NM_006818	ALL1-fused gene from chromosome 1q (AF1Q), mRNA	↓
RDEV201	310	NM_025180	Hypothetical protein FLJ13386 (FLJ13386), mRNA	↓
RDEV204	250	NM_018693	Vitiligo-associated protein VIT-1 (VIT1), mRNA	↓
RDEV222	470	NM_001450	Four and a half LIM domains 2 (FHL2), mRNA	Uniform
RDEV224	440	D43950	mRNA for KIAA0098 protein, partial cds	↓
RDEV250	550	AK001717	cDNA FLJ10855 fis, clone NT2RP4001524	↓↓
RDEV256	450	AF258661	AD034 mRNA, complete cds	↓
RDEV259	360	AK022709	cDNA FLJ12647 fis, clone NT2RM4002013	↑
RDEV261	310	NM_017582	NICE-5 protein (HSA243666), mRNA	↓
RDEV277	460	AF151896	CGI-138 protein mRNA, complete cds	Uniform
RDEV297	400	D26069	mRNA for KIAA0041 gene, partial cds	↓
RDEV301	340	AB044749	mRNA for WDC146, complete cds	Uniform
RDEV310	220	AL050386	mRNA; cDNA DKFZp564G0422 (from clone DKFZp564G0422)	↓
RDEV311	220	AB046793	mRNA for KIAA1573 protein, partial cds	Uniform
RDEV330	350	NM_018243	Hypothetical protein FLJ10849 (FLJ10849), mRNA	↓↓

[a] (↑) General upregulation; (↓) general downregulation; (↓↓) abrupt downregulation.

primers flanking a fragment containing the alternative exon were employed to screen the cDNAs of normal human tissues. PCR yielded two products whose se-

quences revealed the wild-type and alternatively spliced transcripts in brain, colon, heart, kidney, leucocyte, liver, lung, ovary, pancreas, placenta, prostate, skeletal mus-

TABLE 3

List of GenBank Accession Numbers of Other Isolated ESTs

Characteristic	Accession numbers
Thirty-three isolated ESTs showing significant matches with the human EST database[a]	
Six ESTs showing general upregulation	AW661666, AW991226, AW991239, AW991242, BG644290, BG644320
Seven ESTs showing abrupt upregulation	AW991225, AW991235, AW991241, BG644296, BG644299, BG644319, BG644330
Eight ESTs showing general downregulation	AW661663, AW991215, AW991218, AW991240, AW991245, AW991246, BG644297, BG644322
Twelve ESTs showing unaltered expression	AW661657, AW661659, AW661665, AW661667, AW991219, AW991230, AW991232, BG644286, BG644288, BG644298, BG644305, BG644329
Forty-four novel ESTs without any significant match with the database[a]	
Fifteen ESTs showing general upregulation	AW661658, AW661662, AW661664, AW661668, AW991216, AW991220, AW991223, BG644289, BG644295, BG644306, BG644309, BG644323, BG644324, BG644326, BG644327
Twenty-six ESTs showing abrupt upregulation	AW991217, AW991227, AW991228, AW991233, AW991234, AW991236, AW991237, AW991238, AW991243, BG644292, BG644293, BG644300, BG644302, BG644303, BG644307, BG644308, BG644310, BG644311, BG644312, BG644313, BG644314, BG644315, BG644316, BG644318, BG644325, BG644328
One EST showing abrupt downregulation	BG644291
Two ESTs showing unaltered expression	BG644287, BG644294

[a] Sequences of the isolated ESTs were deposited into the GenBank database. Further details are available at the website www.med.nus.edu.sg/mbio/hgl.html.

cle, small intestine, spleen, testis, and thymus (data not shown), indicating ubiquitous expression of both TRIP7 mRNA variants.

A BLAST search of the human genome database revealed high homology of RDEV154 cDNA to the human chromosome 6 working draft sequence and facilitated the mapping of exons and introns to elucidate the genomic organization of TRIP7 (not shown). A search on Genemap revealed genetic markers STSG24893 and WI-12968 that represent TRIP7 on the radiation hybrid (RH) map GB4. Since these two specific markers lie between other markers that have been mapped to 6q14–q15, it was concluded that TRIP7 resides within this locus. Interestingly, the sialin gene maps to this locus and is mutated in sialic acid storage diseases, which are autosomal recessive neurodegenerative disorders.
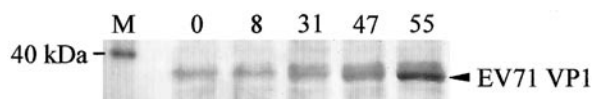

FIG. 4. Western blot analysis of total protein extracts from EV71-infected RD cells reacted against human serum with a high EV71-neutralizing antibody titer (1:128). Lanes 0, 8, 31, 47, and 55 denote the times (in hours) after EV71 infection and reveal ~37-kDa bands of increasing intensity and corresponding to the EV71 VP1 capsid protein. Lane M indicates the 40-kDa band of the protein ladder marker.

The novel RDEV130 sequence encodes a protein similar to vacuolar protein 8

During the course of EV71 infection, the transcription of RDEV130 mRNA in RD cells was relatively uniform (Fig. 3). Two 3′ RACE products of ~300 and ~210 bp corresponding to the 3′ UTR of RDEV130 cDNA were amplified, containing two and one polyadenylation signals, respectively. Their sequences were virtually identical to the 3′ end of the human cDNA FLJ10817 fis, clone NT2RP4001004 (weakly similar to vacuolar protein 8), that originated from NT2 neuronal precursor cells induced with retinoic acid (GenBank Accession No. AK001679). A ~3.0-kb product was amplified by PCR using specific primers 130BB and 130JA designed on the basis of the sequences of the 3′ RACE products and the FLJ10817 clone. Combining the sequences derived from the 3′ RACE and classical PCR fragments produced a cDNA sequence spanning ~3.2 kb that was identical to nt 375–3569 of the FLJ10817 clone, within which was an ORF encoding 682 amino acid residues. A BLAST search with this RDEV130 cDNA against the human genomic contig sequence database revealed its localization to chromosome region 10p12.1. The 682-amino-acid sequence of the RDEV130-encoded protein displayed the highest homology to yeast vacuolar protein 8, human junction plakoglobin or desmoplakin III, human β-catenin, and armadillo segment polarity protein. The RDEV130 amino acid sequence exhibited 97% identity to

```
  1 CAGCATCCAGCGGCGGCGCCAGCAGTTCCAGTCCGTTGCTTTACTTTTTGCTTCACCGACATAGTCATTATGCCGAAGAGAAAGTCTCCA
                                                                           M  P  K  R  K  S  P
 91 GAGAATACAGAGGGCAAAGATGGATCCAAAGTAACTAAACAGGAGCCCACAAGACGGTCTGCCAGATTGTCAGCGAAACCTGCTCCACCA
     E  N  T  E  G  K  D  G  S  K  V  T  K  Q  E  P  T  R  R  S  A  R  L  S  A  K  P  A  P  P
181 AAACCTGAACCCAAACCAAGAAAAACATCTGCTAAGAAAGAACCTGGAGCAAAGATTAGCAGAGGTGCTAAAGGGAAGAAGGAGGAAAAG
     K  P  E  P  K  P  R  K  T  S  A  K  K  E  P  G  A  K  I  S  R  G  A  K  G  K  K  E  E  K
271 CAGGAAGCTGGAAAGGAAGGCACAGAAACTGAATCTGTAGATAACGAGGGAGAATGAATTGTCATGAAAAATTGGGGTTGATTTTATGT
     Q  E  A  G  K  E  G  T  E  N ***
361 ATCTCTTGGGACAACTTTTAAAAGCTATTTTTACCAAGTATTTTGTAAATGCTAATTTTTTAGGACTCTACTAGTTGGCATACGAAATA
451 TATAAGGATGGACATTTTATCGTCTCATAGTCATGCTTTTTGGAAATTTACATCATCCTCAAGTAAAATAAATATCAGTTAAATATTGGA
541 AGCTGTGTGTAAGATTGATTCAGCATTCCATGCACTTGCTTTAAAATTTAGTCCTGTGCATACTGTGGTGTTTTTACTGTGCATATTTGA
631 ATTTTTCATGCAGTTTTTCTAGAGCAATAATCAGTGGTGCTTTTGTACCTAGGTTTTATGTGATTTTAATGAAACATGGATAGTTGTGGC
721 CACCTGCTGACTATTTGTGGTTTAAAATAAAAGGTTTACTTGTCTGCAAAAAAAAAAAAAAAAAAAAAAAA
```

FIG. 5. cDNA and predicted amino acid sequences of RDEV154, a novel alternatively spliced variant of the thyroid receptor interactor TRIP7 (Accession No. AF401520). The 790-nt cDNA incorporates a continuous ORF of 231 nt encoding 77 amino acids. The nuclear localization signal consensus sequences are boxed with broken lines, while the consensus nucleosome core-binding domain is highlighted within a box. The arrow between nt 289 and 290 points to the site at which a 41-bp TRIP7 segment is deleted, leading to a frameshift mutation that culminates in an RDEV154 gene product with a modified and truncated C-terminus. *** Denotes an in-frame termination codon. The italicized nucleotides in boldface in the 5′ UTR include putative binding sites for GC-rich sequence DNA-binding factor, CAP site-binding factor, c-myoglobin, and γ internal ribosome entry. Within the 3′ UTR, single- and double-underlined nucleotides indicate potential mRNA destabilizing motifs (ATTTA or ATTTTA) and the polyadenylation signal (AATAAA), respectively.

a predicted human protein (GenBank Accession No. CAB66793) and identities of 45% and positives of 67% to the CG5155 gene product of *Drosophila* (GenBank Accession No. AAF52507). The RDEV130 gene product was predicted to be a stable, hydrophilic protein of ~75 kDa, with a grand average of hydropathicity of −0.239.

The novel RDEV156 sequence is the putative human homolog of the mouse brain-specific mc7 gene

The transcription of RDEV156 mRNA in RD cells was observed to be stable throughout the course of EV71 infection (Fig. 3). A 442-bp sequence corresponding to RDEV156 cDNA was derived via 3′ RACE and classical PCR. Searching the GenBank database with this cDNA sequence revealed strong homology of ~90% with the 3′ end of murine mRNA for the mc7 protein (GenBank Accession No. AJ278191). Thus, RDEV156 is most likely to represent an EST belonging to the putative human homolog of the mouse mc7 gene. By searching the human genomic contig sequence database, RDEV156 was localized to chromosome region 11p13, coinciding with the loci for acute T-cell leukemia, Wilms tumor type 1, and severe combined immunodeficiency. The RDEV156 gene product was predicted to be an unstable, hydrophilic protein (grand average of hydropathicity of −0.976), with a nuclear localization (reliability of ~70%).

DISCUSSION

In our study using the DD RT–PCR strategy, we characterized an array of known as well as novel genes whose expression profiles were unaltered, upregulated, or downregulated in RD rhabdomyosarcoma cells infected with a neurovirulent EV71 strain. Analysis of the temporal expression of selected genes at various time points following infection provided insights into various genetic phenomena within RD cells in response to the process of progressive infection with EV71. Cellular genes that were uniformly expressed throughout the course of EV71 infection are likely to represent housekeeping genes. A significant proportion of cellular genes (including almost all the novel ESTs) exhibited upregulated expression, which may (1) reflect cellular response events to stress stimuli; (2) allude to cell-related mechanisms of EV71 pathogenesis; and (3) serve as potential markers of EV71 infection. Downregulation of cellular gene expression at transcriptional and translational levels may partly mirror the shutoff of host macromolecular synthesis characteristic of picornavirus infections.

We identified a known gene encoding MAP1B, known to play a critical role in microtubule assembly, whose expression was downregulated. It was previously reported that proteolytic degradation of the related microtubule-associated protein 4 (MAP4) occurs in HeLa cells infected with poliovirus, another enterovirus (Joachims and Etchison, 1992). Poliovirus infection is accompanied by rearrangement of the intermediate filament framework and association of the viral RNA with the cytoskeleton, which may serve as the site for viral RNA replication (Lenk and Penman, 1979; Weed *et al.*, 1985). Hence, a similar phenomenon involving MAP1B may operate in EV71 infection, although the downregulation of MAP1B occurs at the transcriptional level.

MAP1B is actually the earliest microtubule-associated protein to appear during brain development, is most abundant in fetal and neonatal brains (Matus, 1988; Schoenfeld *et al.*, 1989), but is found at only low basal levels in adult brain except in areas with unusually high regenerative activities (Viereck *et al.*, 1989). Such developmental regulation and existence in newly forming neuritic processes suggest a role in neurogenesis and pro-

cess plasticity. MAP1B downregulation may be one of the factors underlying the mechanism of EV71-mediated neurovirulence. MAP1B maps in proximity to the spinal muscular atrophy (SMA) locus at 5q13 (Lien *et al.,* 1991). It is hypothesized that aberrations of MAP1B may lead to defects in the development of the neuron or its structure, resulting in the characteristic degeneration of neurons in SMA patients. This further suggests a possible linkage between the downregulation of MAP1B in EV71 infection with neuromuscular disorders, such as myositis and poliomyelitis-like paralysis, experienced by a subset of EV71-infected patients.

CPE culminating in cell death is likely to be orchestrated by the differential expression of specific genes in response to EV71 infection, including the downregulation of hdlc1 and the upregulation of RTP. Dynein light chain (DLC) is found to be associated with the intermediate chains in both axonemal and cytoplasmic dyneins (King and Patel-King, 1995). By analogy to MAP1B, the downregulation of hdlc1 may play a role in central nervous system diseases induced by EV71 infection. Several studies have described multifunctional roles for DLC, particularly in the regulation of apoptotic processes. DLC has been identified as an inhibitor of neuronal nitric oxide (NO) synthase, a key enzyme in NO biosynthesis (Jaffrey and Synder, 1996). Although NO has antimicrobial activity against bacteria and protozoa, it has an opposing effect in virus infections, especially with neurotropic viruses (Akaike and Maeda, 2000). A probable model is that downregulation of hdlc1 lifts the inhibition of NO synthase, facilitating the generation of peroxynitrite via a radical coupling reaction of NO with superoxide, leading to oxidative tissue injury to the CNS. Such a model is compatible with the neurotropism and neuropathology associated with certain cases of EV71 infection.

Moreover, DLC interacts with IκBα, which inhibits the NFκB family of transcription factors by preventing nuclear translocation of the latter. NFκB is involved in the regulation of genes leading to apoptotic cell death. It is thought that DLC may strengthen the IκBα–c-Rel interaction in order to abort the apoptotic program (Crepieux *et al.,* 1997). A reduction in hdlc1 expression may also signify the easing of IκBα for proteolytic degradation by the 26S proteosome, resulting in the nuclear translocation of NFκB to activate the downstream processes leading to apoptosis. Another apoptotic pathway independent of caspase activity is represented by the diminished interaction between Bim and DLC, which will free Bim to translocate to Bcl-2 and thus neutralize its anti-apoptotic activity (Puthalakath *et al.,* 1999).

DLC also binds the N-terminal domain of nuclear respiratory factor 1 (NRF-1), which acts on genes involved in establishing and maintaining mitochondrial respiratory function for fulfilling cellular energy demands (Scarpulla, 1997). PiC (mitochondrial phosphate carrier) catalyzes the transport of inorganic phosphate from the cytosol into the mitochondrial matrix and is essential for energy metabolism (Kramer, 1996). Hence, downregulation of both genes is likely to drastically disturb cellular metabolism, leading to cellular destruction.

Also variously known as Drg1/Cap43/rit42/TDD5/Ndr1, the RTP gene may also be involved in cell death, as well as in stress responses, androgen responses, hypoxia, atherosclerosis, differentiation, carcinogenesis, and N-myc pathways. RTP mRNA cycles with cell division, peaking at G_1 and G_2–M, with lower expression in S phase (Kurdistani *et al.,* 1998), a phenomenon not observed in tumor cells. The introduction of RTP cDNA into human cancer cells reduces cell growth, suggesting a growth inhibitory role for RTP. In the context of EV71 infection, the upregulation of RTP may inhibit cell growth and ultimately contribute to cell death at the later stages of infection.

CCT4 forms part of a chaperonin complex that binds newly translated cyclin E and mediates its folding into a form that can associate with Cdk2 (Won *et al.,* 1998). This association is a positive regulator of the G_1 to S transition. Thus, low levels of CCT4 will affect the cyclin E–Cdk2 interaction, thereby exerting a negative influence on the cell cycle via G_1 arrest.

A nuclear transport receptor, importin β, interacts with the nuclear pore complex (NPC) to provide a channel where active transport of numerous large particles and certain small molecules from the cytoplasm to the nucleus can proceed in order to support cellular functions. This mechanism permits the import of ribosomal proteins into the nucleus and nucleolus, where they are assembled with rRNA and subsequently exported as ribosomal subunits to the cytoplasm, where they mediate the synthesis of cellular proteins (Jakel and Gorlich, 1998). Histone H1 also enters the nucleus via the same mechanism to maintain the high-order chromatin structure (Jakel *et al.,* 1999). Thus, lower levels of importin β will adversely affect cellular translational efficiency and chromatin structure.

The RDEV154 cDNA represented a novel alternatively spliced transcript of TRIP7, whose expression was downregulated during EV71 infection. TRIP7 is a thyroid receptor interacting protein (TRIP) that requires the presence of thyroid hormone (T$_3$) to interact with the thyroid hormone receptor (Lee *et al.,* 1995). The necessity for thyroid hormone suggests a growth-related mechanism of regulation of TRIP7 to bind to thyroid receptor in order for it to be functional. Liganded thyroid hormone receptors are different in conformation than unliganded receptors (Zhang and Lazar, 2000). This conformational change after ligand binding is responsible for the release of a corepressor complex and is able to recruit a coactivator complex, with the result of activating transcription of the target gene. On the basis of a homology of ~60% with human HMG-17 and the presence of an HMG signature motif, TRIP7 is a member of the HMG class of

nonhistone chromosomal proteins. HMG proteins such as HMG-14 and HMG-17 function by binding to the inner side of nucleosomal DNA to maintain transcribable genes in a unique chromatin conformation so as to improve the efficiency of transcription (Shirakawa *et al.,* 2000). The nuclear localization of HMGs is cell cycle dependent as they are not associated with chromatin during metaphase, and they reenter the nucleus after formation of the nuclear membrane. This reentry is facilitated by an active import system, as seen by the requirement of energy and the participation of importin α (Hock *et al.,* 1998). Phosphorylation of the serine residues in the HMG nucleosomal consensus RRSARLSAK interferes with nuclear localization by either disrupting NLS interactions with importin α or enhancing interactions with exportins (Louie *et al.,* 2000). Furthermore, acetylation of HMGs within conserved lysine residues in the nucleosomal-binding domain as well as the NLS serves to reduce the affinity of HMGs to nucleosomes. Hence, acetylation is crucial in regulating the intranuclear trafficking, targeting, or interaction of HMG proteins with other nuclear factors (Bergel *et al.,* 2000).

Transcripts corresponding to RDEV130 cDNA that exhibited the highest homology to a human clone weakly similar to vacuolar protein 8 were relatively uniform during the course of EV71 infection of RD cells. Vacuolar protein 8 bears similarity to plakoglobins and the β-catenin family, and its main function is to target proteins from the cytoplasm to vacuoles (Fleckenstein *et al.,* 1998). Plakoglobins are common junctional plaque proteins present in desmosomes and intermediate junctions. They also exist in membrane-associated plaques, which are architectural elements in an important strategic position to influence the arrangement and function of the cytoskeleton and cells within tissues. β-Catenins are mainly involved in the regulation of cell adhesion and in signal transduction. They are cytoplasmic when highly phosphorylated and unstable or alternatively translocate to the nucleus when stabilized with a low level of phosphorylation.

RDEV156 cDNA is likely to be the human homolog of the murine mc7 gene, which is predominantly expressed in the mouse brain. Boutou *et al.* (2001) demonstrated early expression of mc7 in neuroblasts and developing neurons and its retention in mature neurons, suggesting a role in neuronal differentiation and maturation in the brain. The mouse mc7 gene is predicted to encode a hydrophilic peripheral protein that possesses zinc finger domains, PEST intramolecular signals for rapid proteolytic degradation by calpains, and the NAP domain belonging to the nucleosome assembly protein family. It has been proposed that mc7 could be a putative binding protein of dystrophin and utrophin C-terminal end in the brain. The product of the Duchenne muscular dystrophy gene, dystrophin, is an intracellular rod-shaped protein that forms part of the dystrophin-associated protein com-

plex (DAPC) that links the cellular actin cytoskeleton with the extracellular matrix (Hemler, 1999). The function of DAPC is best understood in muscle cells, where it plays an important role in stabilizing the muscle as it alternately contracts and relaxes. Interestingly, the expression of RDEV156 mRNA in a wide variety of normal human tissues and cancer cell lines (data not shown) and its relatively constant expression throughout the course of EV71 infection in RD cells imply a housekeeping role for this putative human homolog of mc7.

Concentrating only on viral factors and on the host immune response to viral infection will limit the scope of our understanding of the underlying molecular mechanisms of virus pathogenesis. Differential display RT–PCR (Ryo *et al.,* 2000; Tal-Singer *et al.,* 1998; Zhu *et al.,* 1997) and, more recently, microarray technology (Johannes *et al.,* 1999; Renne *et al.,* 2001) allow us to probe into specific cellular genetic events that occur in response to viral infection, thereby gaining molecular insights into the infection process that will be increasingly important with the completion of the Human Genome Project. Our experimental data have elucidated the differential or unaltered transcription of a wide array of genes of RD malignant muscle cells in response to EV71 infection that constitutes part of the entire repertoire of cellular expression events during the course of such infection. Harnessing the vast information acquired from these expression profiles necessitates several approaches. One strategy is to ascertain whether the observed gene expression profiles are the result of host cell responses to the presence of the virus or the consequence of the interactions between viral proteins and cellular components (Raux *et al.,* 2000). Another aspect is to recognize genes and their products that are critical to the infection process and to determine whether intervention can be achieved at a molecular genetic level. Besides studying the molecular effects of viral infection, this technique also permits the isolation and further characterization of novel and hitherto unknown human genes whose functions are intimately linked with the process of viral infection.

MATERIALS AND METHODS

RD cell culture, EV71 infection, and viable cell count

RD rhabdomyosarcoma cells were propagated in minimum essential medium (MEM), supplemented with 5% fetal bovine serum, HEPES, sodium bicarbonate, and penicillin–streptomycin at 37°C under 5% CO_2 in a humidified incubator. To avoid stimulating rapid cell growth by addition of fresh serum, confluent cells were cultured in MEM with only 2% FCS prior to infection. One batch of uninfected RD cells served as the control, while the other batch was infected with the neurovirulent EV71 strain MS/7423/87 at 10^6 $TCID_{50}$ and incubated at 37°C (Singh *et al.,* 2000). Cell viability and number were assessed by

the trypan blue dye exclusion method for both batches of RD cells at various time points at and after infection.

Differential display RT–PCR

At 0, 8, 31, 47, and 55 h following infection, total RNAs from infected cells were extracted using the SV Total RNA extraction kit (Promega), and RNA concentrations quantitated by UV spectrophotometry at 260 nm. Total RNA (~250 ng each) was reverse-transcribed for first-strand cDNA synthesis using each of the three single-base-anchored oligo(dT) primers (Genhunter). PCR amplifications of each batch of cDNA preparations were performed in duplicate in the presence of >2000 Ci/mmol of $[\alpha\text{-}^{33}P]dATP$ (Amersham Pharmacia) using paired combinations of three anchored primers and eight arbitrary primers from the RNAimage kit 1 (Genhunter), giving a total of 24 primer pairs. PCR thermal cycling conditions were 94°C for 30 s, 40°C for 2 min, and 72°C for 30 s for 40 cycles, followed by 72°C for 5 min and a 4°C hold. The PCR products were electrophoretically separated in 6% polyacrylamide–urea sequencing gels, dried, and visualized by autoradiography. DNA bands of interest were then excised, reamplified under the same conditions, purified, and subjected to direct cycle sequencing using the ABI PRISM BigDye Terminator kit and the ABI PRISM 377 DNA sequencer (Perkin–Elmer) (Chow and Leong, 1999).

Semiquantitative classical RT–PCR

First-strand cDNAs were synthesized by incubating total RNA (25 ng each) with the RNase H^- mutant of Moloney murine leukemia virus reverse transcriptase (Promega) and each gene-specific primer at 42°C for 1 h. Selected gene target fragments were amplified by RT–PCR using individual pairs of gene-specific primers (Table 1) via thermal cycling at 94°C for 30 s, 55°C for 15 s, and 72°C for 30 s through 25 to 34 cycles at the exponential phase of amplification, determined empirically in each case. RT–PCR products were electrophoresed in 1.4% agarose gels, digitized images were recorded using the Kodak DC120 digital camera, and target bands analyzed by densitometric scanning with the GS-700 Imaging Densitometer and the Quantity One software (Bio–Rad).

Real-time RT–PCR

Total RNA (0.1 μg each) from EV71-infected cells at various time points was reverse-transcribed using oligo(dT) primers. Real-time RT–PCR was performed for 16 selected genes using gene-specific primer pairs (Table 1), iCycler iQ SG-1 (1×) reaction mix (Bio–Rad), and *Taq* polymerase (Promega). The Real-time iCycler iQ system (Bio–Rad) was used to record the increase in SYBR-green signal at the end of each extension period. For each sample, the threshold cycle (C_T) was analyzed for the gene of interest and for the sarcosin housekeeping gene using the iCycler analysis software, and the difference between their C_T values (ΔC_T) was determined. For each gene of interest, the infected sample at 0 h was chosen as the reference, and its ΔC_T value subtracted from the ΔC_T values of infected samples at other time points in order to find the $\Delta\Delta C_T$ or D value for each sample. Finally, the 2^{-D} value was calculated to obtain its relationship with respect to the reference sample in order to reflect the relative expression level for each sample.

Western blot analysis

RD cells infected with EV71 at various time points were lysed using cold lysis buffer containing 3 mM $CaCl_2$, 2 mM $MgCl_2$, 150 mM NaCl, 3 mM dithiothreitol, 0.02% Nonidet P-40, and protease inhibitor cocktail. Cell lysates (80 μg each) were separated by SDS–PAGE alongside BENCHMARK protein ladder markers (Gibco BRL). The separated proteins were transferred to polyvinylidine difluoride membranes, sequentially reacted with human serum containing a high titer of EV71 neutralizing antibodies (1:128), goat antihuman IgG and IgM (heavy and light chains), biotin-conjugated secondary antibodies (Pierce), and streptavidin alkaline phosphatase (Bio–Rad). Specific immunoreactive bands were identified by color reaction using NBT and BCIP substrates (Sim and Chow, 1999).

Molecular analyses of RDEV154, RDEV130, and RDEV156 cDNAs and gene products

To assess the specificity and abundance of tissue expression, gene-specific primers were employed in the PCR amplification of a wide range of normal human tissues using Multiple Tissue cDNA (MTC) panel kits (Clontech) and of several cancer cell lines. Rapid amplification of cDNA ends (RACE) was performed using gene-specific primers with MOLT-4 human lymphoblastic leukemia Marathon-Ready cDNA (Clontech) or with the Switch Mechanism at the 5′ end of the RNA Transcript (SMART) RACE kit (Clontech). Amplified products that were not amenable to direct cycle sequencing were subjected to TA cloning using the pGEM-T Easy Vector system (Promega). Recombinant plasmids were extracted and purified using the QIAprep Spin Miniprep kit (Qiagen) before subjecting the inserts to automated sequencing using vector-specific primers PH1001 and PH1002. Computational analyses of nucleotide and amino acid sequence data were achieved using websites and bioinformatics tools, including BCM Search Launcher, BLAST, CLUSTALW, DNASIS, ExPasy, GenBank, Genemap, MBS Translator, Motif Finder, OMIM, ORF Finder, Plot Structure, PROSITE, ProtParam, and PSORT.

ACKNOWLEDGMENTS

REFERENCES

Akaike, T., and Maeda, H. (2000). Nitric oxide and virus infection. *Immunology* **101,** 300–308.

Alfonso, P. J., Crippa, M. P., Hayes, J. J., and Bustin, M. (1994). The footprint of chromosomal proteins HMG-14 and HMG-17 on chromatin subunits. *J. Mol. Biol.* **236,** 189–198.

Bergel, M., Herrera, J. E., Thatcher, B. J., Prymakowska-Bosak, M., Vassilev, A., Nakatani, Y., Martin, B., and Bustin, M. (2000). Acetylation of novel sites in the nucleosomal binding domain of chromosomal protein HMG-14 by p300 alters its interaction with nucleosomes. *J. Biol. Chem.* **275,** 11514–11520.

Boutou, E., Matsas, R., and Mamalaki, A. (2001). Isolation of a mouse brain cDNA expressed in developing neuroblasts and mature neurons. *Mol. Brain Res.* **86,** 153–167.

Chow, V. T. K., Quek, H. H., and Tock, E. P. C. (1993). Alternative splicing of the p53 tumor suppressor gene in the Molt-4 T-lymphoblastic leukemia cell line. *Cancer Lett.* **73,** 141–148.

Chow, V. T. K., and Leong, P. W. F. (1999). Complete nucleotide sequence, genomic organization and phylogenetic analysis of a novel genital human papillomavirus type, HLT7474-S. *J. Gen. Virol.* **80,** 2923–2929.

Crépieux, P., Kwon, H., Leclerc, N., Spencer, W., Richard, S., Lin, R. T., and Hiscott, J. (1997). IκBα physically interacts with a cytoskeleton-associated protein through its signal response domain. *Mol. Cell. Biol.* **17,** 7375–7385.

Fleckenstein, D., Rohde, M., Klionsky, D. J., and Rudiger, M. (1998). Yel013p (Vac8p), an armadillo repeat protein related to plakoglobin and importin alpha is associated with the yeast vacuole membrane. *J. Cell Sci.* **111,** 3109–3118.

Gilbert, G. L., Dickson, K. E., Waters, M. J., Kennett, M. L., Land, S. A., and Sneddon, M. (1988). Outbreak of enterovirus 71 infection in Victoria, Australia, with a high incidence of neurologic involvement. *Pediatr. Infect. Dis. J.* **7,** 484–488.

Hemler, M. E. (1999). Dystroglycan versatility. *Cell* **97,** 543–546.

Hock, R., Scheer, U., and Bustin, M. (1998). Chromosomal proteins HMG-14 and HMG-17 are released from mitotic chromosomes and imported into the nucleus by active transport. *J. Cell Biol.* **143,** 1427–1436.

Jaffrey, S. R., and Synder, S. H. (1996). PIN: An associated protein inhibitor of neuronal nitric oxide synthase. *Science* **274,** 774–777.

Jäkel, S., and Görlich, D. (1998). Importin β, transportin, RanBP5 and RanBP7 mediate nuclear import of ribosomal proteins in mammalian cells. *EMBO J.* **17,** 4491–4502.

Jäkel, S., Albig, W., Kutay, U., Bischoff, F. R., Schwamborn, K., Doenecke, D., and Görlich, D. (1999). The importin β/importin 7 heterodimer is a functional nuclear import receptor for histone H1. *EMBO J.* **18,** 2411–2423.

Joachims, M., and Etchison, D. (1992). Poliovirus infection results in structural alteration of a microtubule-associated protein. *J. Virol.* **66,** 5797–5804.

Johannes, G., Carter, M. S., Eisen, M. B., Brown, P. O., and Sarnow, P. (1999). Identification of eukaryotic mRNAs that are translated at reduced cap binding complex eIF4F concentrations using a cDNA microarray. *Proc. Natl. Acad. Sci. USA* **96,** 13118–13123.

King, S. M., and Patel-King, R. S. (1995). The $M_r = 8,000$ and 11,000 outer arm dynein light chains from *Chlamydomonas* flagella have cytoplasmic homologues. *J. Biol. Chem.* **270,** 11445–11452.

Koonce, M. P., and Tikhonenko, I. (2000). Functional elements within the dynein microtubule-binding domain. *Mol. Biol. Cell.* **11,** 523–529.

Kramer, R. (1996). Structural and functional aspects of the phosphate carrier from mitochondria. *Kidney Int.* **49,** 947–952.

Kurdistani, S. K., Arizti, P., Reimer, C. L., Sugrue, M. M., Aaronson, S. A., and Lee, S. W. (1998). Inhibition of tumor cell growth by RTP/rit42 and its responsiveness to p53 and DNA damage. *Cancer Res.* **58,** 4439–4444.

Lee, J. W., Choi, H. S., Gyuris, J., Brent, R., and Moore, D. D. (1995). Two classes of proteins dependent on either the presence or absence of thyroid hormone for interaction with the thyroid hormone receptor. *Mol. Endocrinol.* **9,** 243–254.

Lenk, R., and Penman, S. (1979). The cytoskeletal framework and poliovirus metabolism. *Cell* **16,** 289–301.

Liang, P., and Pardee, A. B. (1992). Differential display of eukaryotic messenger RNA by means of the polymerase chain reaction. *Science* **257,** 967–971.

Liang, P., and Pardee, A. B. (1995). Recent advances in differential display. *Curr. Opin. Immunol.* **7,** 274–280.

Lien, L. L., Boyce, F. M., Kleyn, P., Brzustowicz, L. M., Menninger, J., Ward, D. C., Gilliam, T. C., and Kunkel, L. M. (1991). Mapping of human microtubule-associated protein 1B in proximity to the spinal muscular atrophy locus at 5q13. *Proc. Natl. Acad. Sci. USA* **88,** 7873–7876.

Louie, D. F., Gloor, K. K., Galasinski, S. C., Resing, K. A., and Ahn, N. G. (2000). Phosphorylation and subcellular redistribution of high mobility group proteins 14 and 17, analyzed by mass spectrometry. *Protein Sci.* **9,** 170–179.

Mattaj, I. W., and Englmeier, L. (1998). Nucleocytoplasmic transport: The soluble phase. *Annu. Rev. Biochem.* **67,** 265–306.

Matus, A. (1988). Microtubule-associated proteins: Their potential role in determining neuronal morphology. *Annu. Rev. Neurosci.* **11,** 29–44.

Puthalakath, H., Huang, D. C., O'Reilly, L. A., King, S. M., and Strasser, A. (1999). The proapoptotic activity of the Bcl-2 family member Bim is regulated by interaction with the dynein motor complex. *Mol. Cell* **3,** 287–296.

Raux, H., Flamand, A., and Blondel, D. (2000). Interaction of the rabies virus P protein with the LC8 dynein light chain. *J. Virol.* **74,** 10212–10216.

Renne, R., Barry, C., Dittmer, D., Compitello, N., Brown, P. O., and Ganem, D. (2001). Modulation of cellular and viral gene expression by the latency-associated nuclear antigen of Kaposi's sarcoma-associated herpesvirus. *J. Virol.* **75,** 458–468.

Ryo, A., Suzuki, Y., Arai, M., Kondoh, N., Wakatsuki, T., Hada, A., Shuda, M., Tanaka, K., Sato, C., Yamamoto, M., and Yamamoto, N. (2000). Identification and characterization of differentially expressed mRNAs in HIV type 1-infected human T cells. *AIDS Res. Hum. Retroviruses* **16,** 995–1005.

Scarpulla, R. C. (1997). Nuclear control of respiratory chain expression in mammalian cells. *J. Bioenerg. Biomembr.* **29,** 109–119.

Schoenfeld, T. A., McKerracher, L., Obar, R., and Vallee, R. B. (1989). MAP1A and MAP1B are structurally related microtubule associated proteins with distinct developmental patterns in the CNS. *J. Neurosci.* **9,** 1712–1730.

Shih, S. R., Li, Y. S., Chiou, C. C., Suen, P. C., Lin, T. Y., Chang, L. Y., Huang, Y. C., Tsao, K. C., Ning, H. C., Wu, T. Z., and Chan, E. C. (2000). Expression of capsid protein VP1 for use as antigen for the diagnosis of enterovirus 71 infection. *J. Med. Virol.* **61,** 228–234.

Shirakawa, H., Herrera, J. E., Bustin, M., and Postnikov, Y. (2000). Targeting of high mobility group-14/-17 proteins in chromatin is independent of DNA sequence. *J. Biol. Chem.* **275,** 37937–37944.

Sim, D. L. C., and Chow, V. T. K. (1999). The novel human HUEL (C4orf1) gene maps to chromosome 4p12–p13 and encodes a nuclear protein containing the nuclear receptor interaction motif. *Genomics* **59,** 224–233.

Singh, S., Chow, V. T. K., Chan, K. P., Ling, A. E., and Poh, C. L. (2000). RT-PCR, nucleotide, amino acid and phylogenetic analyses of enterovirus type 71 strains from Asia. *J. Virol. Methods* **88,** 193–204.

Tal-Singer, R., Podrzucki, W., Lasner, T. M., Skokotas, A., Leary, J. J.,

Fraser, N. W., and Berger, S. L. (1998). Use of differential display reverse transcription-PCR to reveal cellular changes during stimuli that results in herpes simplex virus type 1 reactivation from latency: Upregulation of immediate-early cellular response genes TIS7, interferon, and interferon regulatory factor-1. *J. Virol.* **72,** 1252–1261.

Viereck, C., Tucker, R. P., and Matus, A. (1989). The adult rat olfactory system expresses microtubule-associated proteins found in the developing brain. *J. Neurosci.* **9,** 3547–3557.

Weed, H. G., Krochmalnic, G., and Penman, S. (1985). Poliovirus metabolism and the cytoskeletal framework: Detergent extraction and resinless section electron microscopy. *J. Virol.* **56,** 549–557.

Won, K. A., Schumacher, R. J., Farr, G. W., Horwich, A. L., and Reed, S. I. (1998). Maturation of human cyclin E requires the function of eukaryotic chaperonin CCT. *Mol. Cell. Biol.* **18,** 7584–7589.

Yan, J. J., Wang, J. R., Liu, C. C., Yang, H. B., and Su, I. J. (2000). An outbreak of enterovirus 71 infection in Taiwan 1998: A comprehensive pathological, virological, and molecular study on a case of fulminant encephalitis. *J. Clin. Virol.* **17,** 13–22.

Zhang, J., and Lazar, M. A. (2000). The mechanism of action of thyroid hormones. *Annu. Rev. Physiol.* **62,** 439–466.

Zhu, H., Cong, J. P., and Shenk, T. (1997). Use of differential display analysis to assess the effect of human cytomegalovirus infection on the accumulation of cellular RNAs: Induction of interferon-responsive RNAs. *Proc. Natl. Acad. Sci. USA* **94,** 13985–13990.